

# Characterizing a permanent magnet using diamond NV center electron spin magnetometry

## Research Practicum

Lucas de Kam (4668448)  
Kate McDonnell (4663993)

Delft, 07/06/2021  
Teacher: T. van der Sar  
Supervisors: B. Simon & M. Bolhuis

# Contents

Abstract . . . . .	iii
1. Introduction . . . . .	1
2. Theory . . . . .	2
2.1 NV centers in a diamond crystal . . . . .	2
2.2 Spin state and photoluminescence . . . . .	2
2.3 Spin magnetometry . . . . .	3
2.4 Field of a magnetic dipole . . . . .	5
3. Experimental methods . . . . .	7
3.1 The setup . . . . .	7
3.2 Data collection . . . . .	8
3.2.1 Varying the distance . . . . .	8
3.2.2 Varying the angle . . . . .	8
3.3 Data analysis . . . . .	9
3.3.1 Magnitude of the magnetic field . . . . .	9
3.3.2 Direction of the magnetic field . . . . .	10
4. Results and Discussion . . . . .	11
4.1 Magnitude against distance . . . . .	11
4.2 Magnitude against angle . . . . .	13
4.3 Direction . . . . .	13
5. Conclusion . . . . .	15
References . . . . .	16
Appendix . . . . .	17

## **Abstract**

The aim of this project is to characterize the magnetic field of a small permanent magnet using NV center magnetometry. NV center magnetometry is based on measuring electron spin resonance (ESR) frequencies of nitrogen vacancy (NV) defects in diamond using a fluorescence microscope. The ESR frequencies are directly related to the external magnetic field.

The experiment consisted of varying the distance of the permanent magnet to the diamond while keeping the angle constant, and varying the angle of the permanent magnet to the diamond at a fixed distance. The magnitude of the B-field, calculated directly from the ESR frequencies, was compared to the theoretical result from classical electromagnetism. The direction of the B-field was obtained by fitting the components of the vector magnetic field.

Computing the magnitude of the magnetic field directly from the ESR frequencies proved to be a reliable method. The measured dependence of magnitude on distance and angle corresponded well to the prediction from classical electromagnetism. On the other hand, fitting the components of the vector magnetic field to the ESR frequencies was highly dependent on the initial values used in the fitting procedure. Nevertheless, for appropriate guesses, the fitted magnetic field was very similar to the field calculated from the theory.

The largest inaccuracies of this experiment were due to uncertainties in the placement of the magnet with respect to the diamond crystal. Eliminating these uncertainties would improve the reliability of the found results. For future studies the fitting procedure for fitting the components of the vector magnetic field could also be improved.

# **1. Introduction**

Over the past couple of decades, nitrogen-vacancy centers (NV centers) in diamond have been explored as a way to measure magnetic fields with high sensitivity [1]. One advantage of NV centers is that they can be used at room temperature. In contrast, conventional magnetometers such as those based on superconducting quantum interference devices (SQUIDs) need to be cooled with liquid helium [2], which complicates logistics.

Applications of NV center magnetometry show promising results. In a recent study, NV centers were used to measure the concentration of magnetic nanoparticles in biological tissue, with the aim to develop new methods for cancer treatment and diagnosis [3].

In this project, we will use NV center magnetometry to characterize the magnetic field of a small permanent magnet. In particular, the aim is to determine how the magnitude of the magnetic field depends on the distance from the magnet, and on the angle to the magnet axis. We also determine the direction of the magnetic field in several locations around the magnet using a fitting procedure for the vector magnetic field.

In Chapter 2, Theory, we discuss the relevant theory to grasp the concept of NV magnetometry. Then in Chapter 3, Experimental methods, we explain how we set up the experiment to answer the three subquestions. In Chapter 4, Results and Discussion, we present the results of the experiments including a discussion of the obtained results and what improvements can be made. Then finally in Chapter 5, Conclusion, the most important results and discussion points are summarized to give an answer to the main question of this report.

This experiment is part of the course Research Practicum which is a part of the bachelor's degree Applied Physics at the TU Delft.

## 2. Theory

Here, we introduce the theory needed to understand our methods and results. First, we give a general introduction of NV centers in diamond. Then, we explain how the spin state of NV centers can be measured, and how this can be used to measure an external magnetic field. Finally, we give a short overview of the relevant theory for the field of a magnetic dipole.

### 2.1. NV centers in a diamond crystal

In the crystal structure of diamond, a nitrogen vacancy (NV) center is a lattice defect which consists of a nitrogen atom, instead of a carbon atom, with a vacancy next to it. Since the diamond crystal has a set symmetry, there are four possible ways in which the NV center axis can be oriented in the crystal (Figure 1). The angle of the NV center axis to the [001] normal vector (the  $z$ -axis in Figure 1) can be either approximately 54.7 or 125.3 degrees.

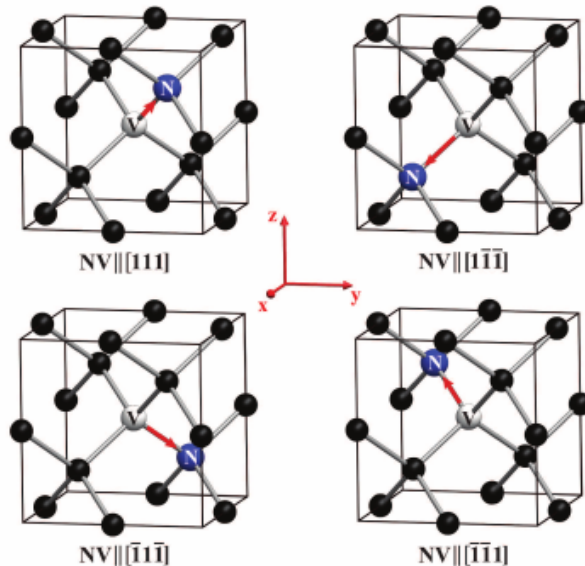


**Figure 1:** Four possible NV center axis orientations. The directions of the NV center axes are denoted using Miller indices and are indicated by red arrows in the crystals. The  $z$ -axis points upwards, so the [001] surface is the top surface. Figure taken from [4].

### 2.2. Spin state and photoluminescence

The pair of electrons in the NV center has a combined spin  $S = 1$ . Therefore it has three different spin states  $m_s$ , namely  $m_s = -1, 0$  and  $+1$ .

NV centers can be excited using a green laser with a wavelength of 532 nm in such a way that the spin is preserved. From the excited state, decay to the ground state can occur in two ways. The first is the radiative decay in which the spin is again preserved and the NV center emits red photons. The second decay is called the non-radiative decay. This only happens to  $m_s = \pm 1$  states and it does not preserve spin, as it decays via a metastable state to the  $m_s = 0$  ground state (Figure 2) [5].

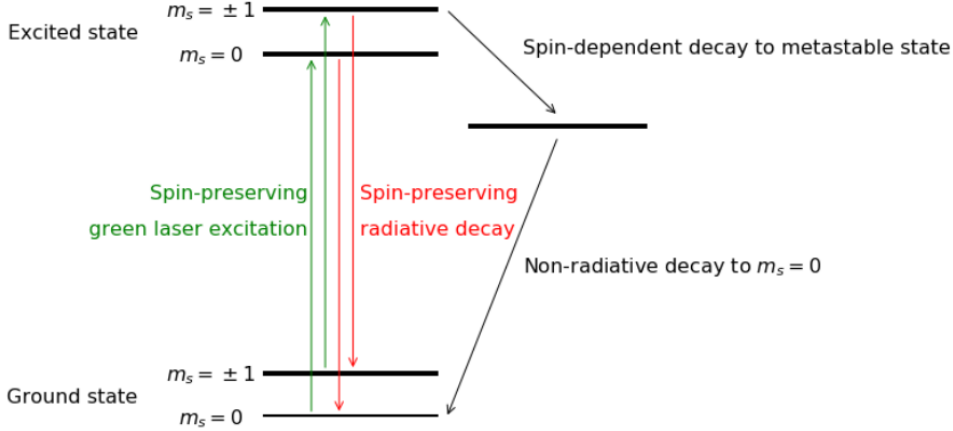


**Figure 2:** Initialization process of the spin states  $m_s = 0, -1, +1$ . Spin-preserving excitation by a green laser followed by spin-preserving radiative decay and non-spin-preserving non-radiative decay via a metastable state. Figure taken from [5].

This property can be used to initialize (polarize) the NV centers into the  $m_s = 0$  state. By continuous excitation with the green laser, more and more centers in an  $m_s = \pm 1$  state decay to an  $m_s = 0$  state by non-radiative decay. They stay in this state due to the fact that the radiative decay preserves spin.

Importantly, the number of photons emitted by the NV centers (their photoluminescence) gives information about their spin state. If all centers are polarized in the  $m_s = 0$  state, all the decay is radiative and spin-preserving, so photoluminescence is high. On the other hand, if many centers are in the  $m_s = \pm 1$  state, some of the decay is non-radiative, and photoluminescence will be lower.

### 2.3. Spin magnetometry

The energies of the different spin states ( $m_s = -1, 0$  and  $+1$ ) depend on the external magnetic field (this is called the Zeeman effect). An external small-amplitude oscillating magnetic field can drive transitions between these energy levels with  $\Delta m_s = 1$ . The frequency of the oscillating field is proportional to the transition energy. As a result, the frequencies that can drive  $\Delta m_s = 1$  transitions are directly related to the (stationary) external magnetic field. These frequencies are called electron spin resonance (ESR) frequencies.

We can determine the energy levels by diagonalizing the Hamiltonian for the NV center spin, which is given in units of GHz by [5]

$$H = DS_z^2 + \gamma \mathbf{B} \cdot \mathbf{S}, \quad (1)$$

where  $D$  is the zero-field splitting, which has a theoretical value of 2.87 GHz;  $\gamma = 28$  GHz/T the electron gyromagnetic ratio and  $\mathbf{B}$  the vector magnetic field in T. The spin vector is  $\mathbf{S} = S_x \hat{\mathbf{x}} + S_y \hat{\mathbf{y}} + S_z \hat{\mathbf{z}}$ ;  $S_x$ ,  $S_y$  and  $S_z$  are the Pauli spin matrices for a spin 1. The  $z$ -axis is defined to be along the NV center axis. Figures 3A and 3C show the eigenenergies of the Hamiltonian for a magnetic field respectively parallel and perpendicular to the NV center axis.

The ESR frequencies are now simply given by the absolute difference between states that

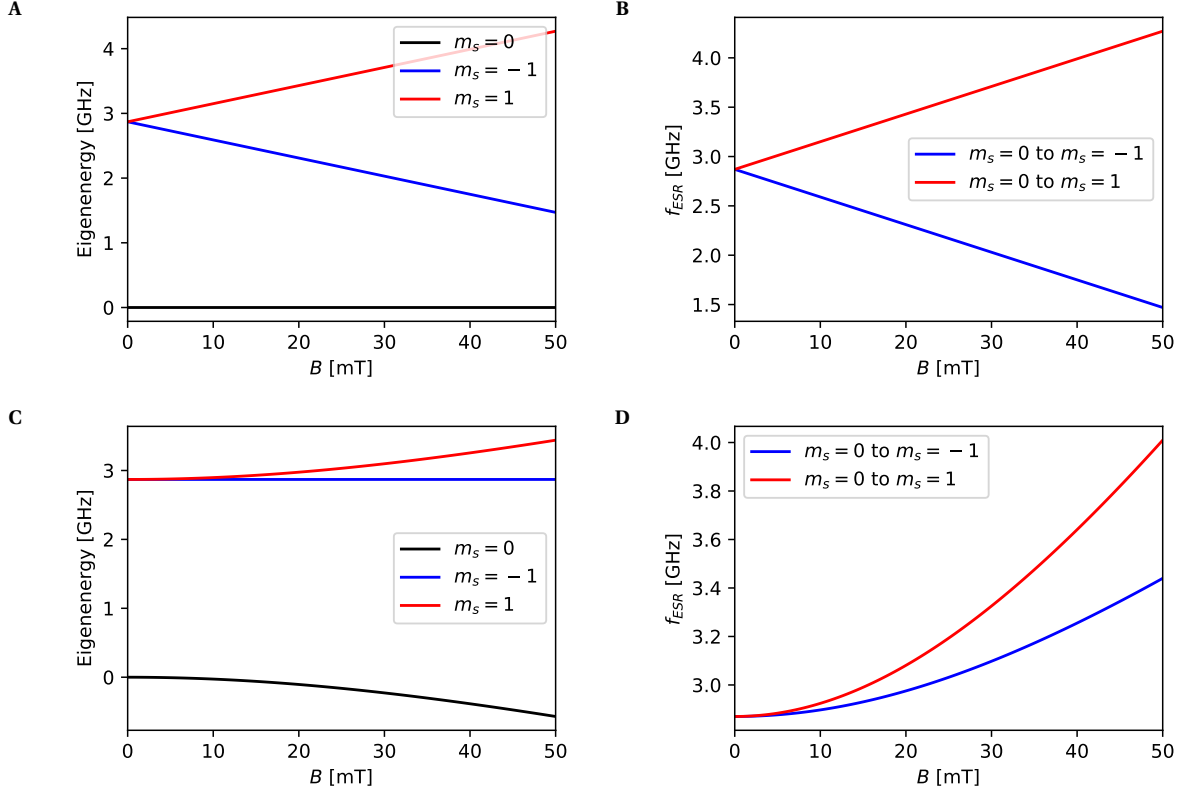


**Figure 3:** Eigenenergies of the NV center Hamiltonian and electron spin resonance (ESR) frequencies plotted against the magnitude of the magnetic field, for different orientations of the magnetic field. **A:** Eigenfrequencies for magnetic field along the NV center axis. **B:** ESR frequencies for magnetic field along the NV center axis. **C:** Eigenfrequencies for magnetic field perpendicular to the NV center axis. **D:** ESR frequencies for magnetic field perpendicular to the NV center axis.

differ by  $\Delta m_s = 1$ . Figures 3B and 3D show the ESR frequencies for a parallel and perpendicular magnetic field, respectively.

Consider the situation where all NV centers are polarized in the  $m_s = 0$  state using the green laser. If the frequency of the oscillating magnetic field is then set equal to an ESR frequency, some NV centers will transition to the  $m_s = \pm 1$  states, and this decreases photoluminescence temporarily. On the other hand, if the frequency is not equal to an ESR frequency, the NV centers remain in the  $m_s = 0$  state and photoluminescence remains high.

This contrast makes it possible to measure ESR frequencies by sweeping over a range of frequencies and measuring the photoluminescence of the diamond crystal. The frequencies at which the intensity drops, are ESR frequencies. Determining the range of the frequency sweep is detailed in the Experimental Methods (Chapter 3).

Figure 3 shows that different orientations of the  $B$ -field with respect to the NV center axis give different ESR frequencies. For any  $B \neq 0$ , ESR frequencies for a certain NV center orientation come in pairs. Since there are four different orientations (families), at most eight different ESR frequencies can be measured in a frequency sweep. For a certain family, the lower ESR frequency is called  $f_l$  and the upper is called  $f_u$ . The magnitude of the magnetic

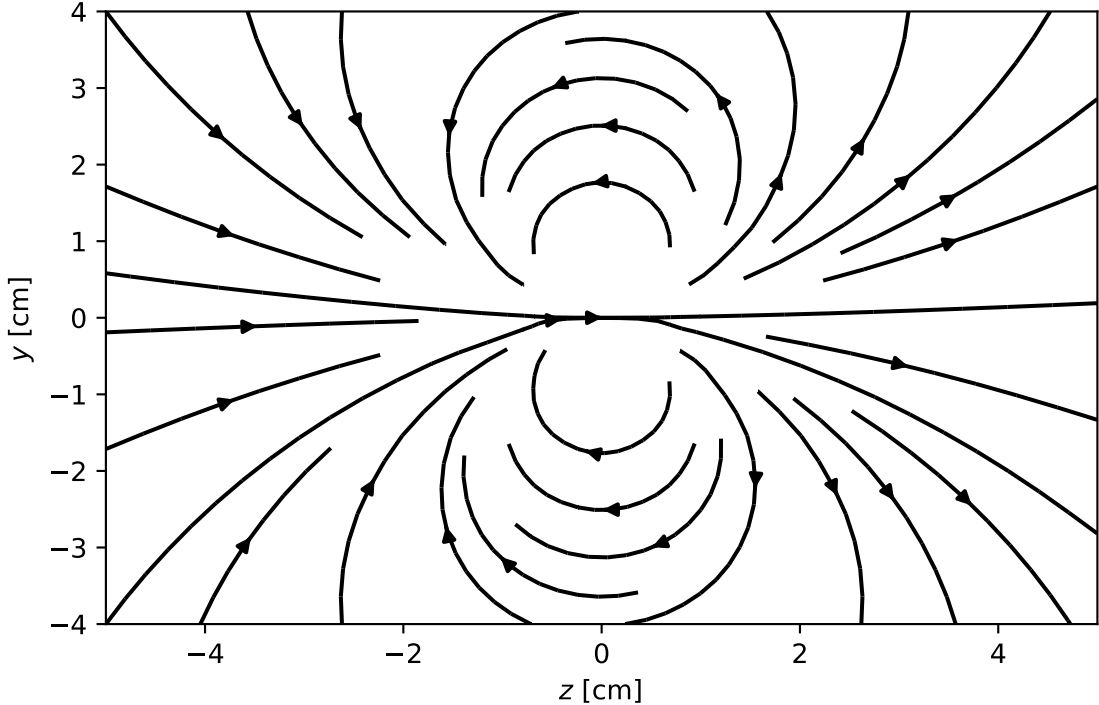


**Figure 4:** Magnetic field lines in the  $(z, y)$ -plane for an ideal magnetic dipole  $\mathbf{m} = 1.500\hat{z}$  located at the origin. The field lines are plotted using Equation 4.

field  $B$  can be expressed in terms of  $f_1$  and  $f_u$  as [5]

$$B = \frac{1}{\gamma\sqrt{3}} \sqrt{f_u^2 + f_1^2 - f_u f_1 - D^2}. \quad (2)$$

## 2.4. Field of a magnetic dipole

An ideal magnetic dipole has a magnetic moment  $\mathbf{m}$  pointing along the magnet axis. The magnitude of the magnetic moment, denoted  $m$ , can be calculated as follows [5],

$$m = \iiint_V M dV. \quad (3)$$

Here  $M$  is the magnetization (in A/m) and  $V$  the volume of the magnet. The magnetic field  $\mathbf{B}$  of a dipole located at the origin can be calculated using  $\mathbf{m}$  [6],

$$\mathbf{B}(\mathbf{r}) = \frac{\mu_0}{4\pi} \frac{3\mathbf{r}(\mathbf{m} \cdot \mathbf{r}) - \mathbf{m}}{r^3}, \quad (4)$$

where  $\mu_0$  is the vacuum permeability constant and  $\mathbf{r}$  is the position with respect to the center of the dipole. In Figure 4 the magnetic field for an ideal dipole magnet has been depicted. From Equation 4, it can be derived that the magnitude  $B$  changes with distance along the magnet axis (the  $z$ -axis) as

$$B(z) = \frac{m\mu_0}{2\pi} \frac{1}{z^3}. \quad (5)$$

Also, when going around the magnet at a fixed distance  $R$ , the magnitude of the magnetic field depends on the angle  $\theta$  to the z-axis as

$$B(\theta) = \frac{m\mu_0}{4\pi R^3} \sqrt{3 \cos^2 \theta + 1}. \quad (6)$$

### 3. Experimental methods

In this section we will first discuss the setup of the experiment, and define a coordinate system. Then we will describe how we used frequency sweeps to collect the ESR frequency data. We gathered two sets of data: one where we varied the distance between the diamond and the magnet, and one where we varied the angle of the magnet with respect to the diamond surface. At the end of this section, we describe how we analyzed the data to determine the actual magnitude and direction of the magnetic field.

#### 3.1. The setup

To measure the ESR frequencies of the NV centers, we used a fluorescence microscope (Figure 5). A green laser with a wavelength of 532 nm is sent through a microscope objective to the diamond, using a dichroic mirror. To create the oscillating magnetic field, a wire placed on the diamond crystal surface is connected to a generator that creates a microwave current, which in turn induces the desired oscillating magnetic field. The red photons emitted by the diamond are transmitted by the dichroic mirror to fall on a CMOS camera.

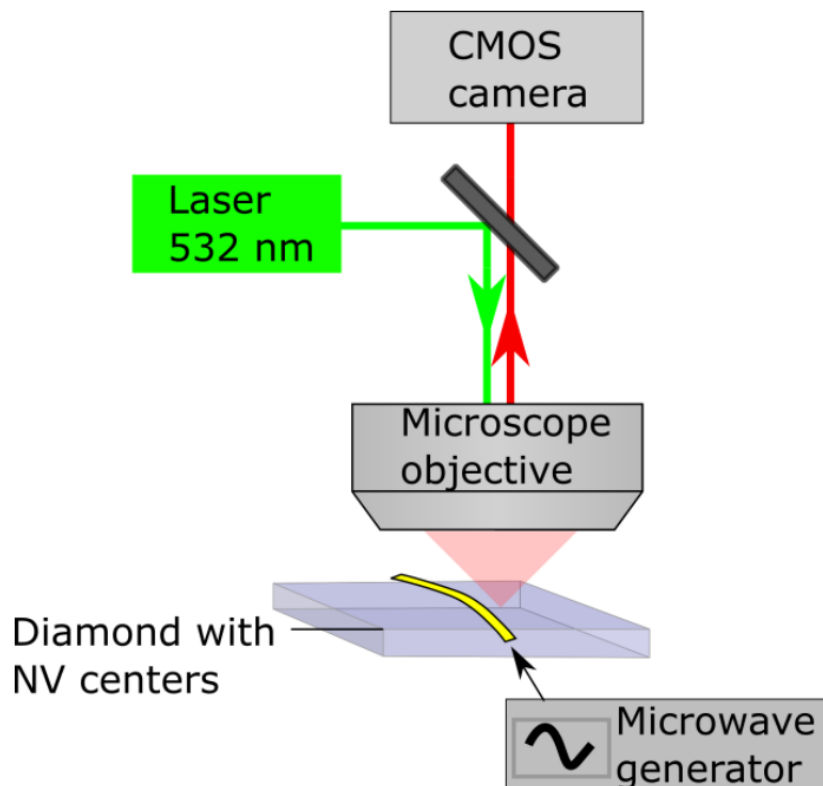


**Figure 5:** A schematic representation of the fluorescence microscope. Depicted are all the components of the microscope including the light paths of the green laser and red photons. Figure taken from [5].

To measure the amount of light the NV centers emitted, the number of pixels of the CMOS camera image that were turned on (active) were counted. To reduce the amount of noise, we cropped the image to include only the light spot being emitted by the diamond.

The small permanent cylindrical magnet that we characterized had a radius of 5 mm, a length of 2 cm and a constant magnetization  $M = 0.955 \cdot 10^6$  A/m [7]. By equation 3, the magnetic moment  $m$  is simply  $M$  times the volume:

$$m = \pi r^2 LM \approx 1.500 \text{ A m}^2. \quad (7)$$

Figure 6 shows the definition of the coordinate systems of the magnet and diamond. For the coordinate system of the magnet, the magnet axis is taken as the  $z$ -axis; the magnet is located at the origin. When rotating the magnet (Figure 6), we define the plane of rotation to be the  $(z, y)$ -plane. The angle between the normal of the diamond surface and the  $z$ -axis is denoted  $\theta$ .

For the coordinate system of the diamond crystal, coordinates are denoted using primes ('). The normal vector to the diamond surface pointing *away* from the magnet defines the  $z'$ -axis, which coincides with the magnet  $z$ -axis when  $\theta = 0^\circ$ . The  $y'$ -axis is perpendicular to the  $z'$ -axis such that the  $(z, y)$  plane coincides with the  $(z', y')$ -plane if the magnet is mounted at the same height as the diamond crystal. The diamond is located at the origin of this coordinate system.

### 3.2. Data collection

Before the measurement, a camera exposure time and a range and step size for the frequency sweep were selected. Camera exposure time should be as low as possible without missing frames. We chose the frequency range as to include all expected ESR frequencies, with a resolution of 50 steps per interval of 0.1 GHz. Then, we let the microwave generator sweep over the selected frequency range, and measured the number of active pixels in each frequency step. This was repeated 50 times, and all the results were averaged. The total number of active pixels was plotted against the microwave frequency to get a frequency spectrum. A Lorentzian fit was used to determine the center of each intensity dip (peak). The frequency of the center of the peak is then the measured ESR frequency.

#### 3.2.1. Varying the distance

For varying the distance between magnet and diamond, we mounted the permanent magnet with its axis (the  $z$ -axis) perpendicular to the surface of the diamond ( $\theta = 0$ ), at roughly the same height as the crystal. The initial distance between the center of the magnet and the diamond was measured using a ruler to be roughly 5.0 cm. We estimate an uncertainty of this measurement of 0.3 cm.

The magnet was then moved closer to the diamond in steps of 3 mm; when we got closer to the magnet we changed to steps of 2 mm. This was done to account for the faster rate of change of the B-field magnitude at smaller distances (Equation 5). Each step, a frequency sweep was carried out to measure the ESR frequencies. The distance between steps was read off from a scale on the magnet stand with high accuracy. Within 2.5 cm of the magnet, the frequency spectra became very noisy, and getting correct Lorentzian fits was not feasible.

#### 3.2.2. Varying the angle

For this round of measurements, the magnet was fixed on a rotating stand with a dial to read off the angle  $\theta$  (Figure 6). The center of the magnet was located at a distance  $R = 3.2$

$\text{cm} \pm 0.3 \text{ cm}$  (ruler measurement), again at roughly the same height as the diamond crystal. However, the setup was such that we could only fix the magnet stand with one screw. This made it difficult to make sure that the magnet was perfectly perpendicular to the diamond surface for  $\theta = 0$ .

The magnet was rotated counterclockwise from the perspective in Figure 6. The angle was varied between  $0^\circ$  and  $90^\circ$  in steps of  $10^\circ$ , with  $0^\circ$  being perpendicular to the diamond surface. Again, the ESR frequencies were measured at each step. We also did two extra measurements arbitrarily at  $35^\circ$  and  $55^\circ$ .

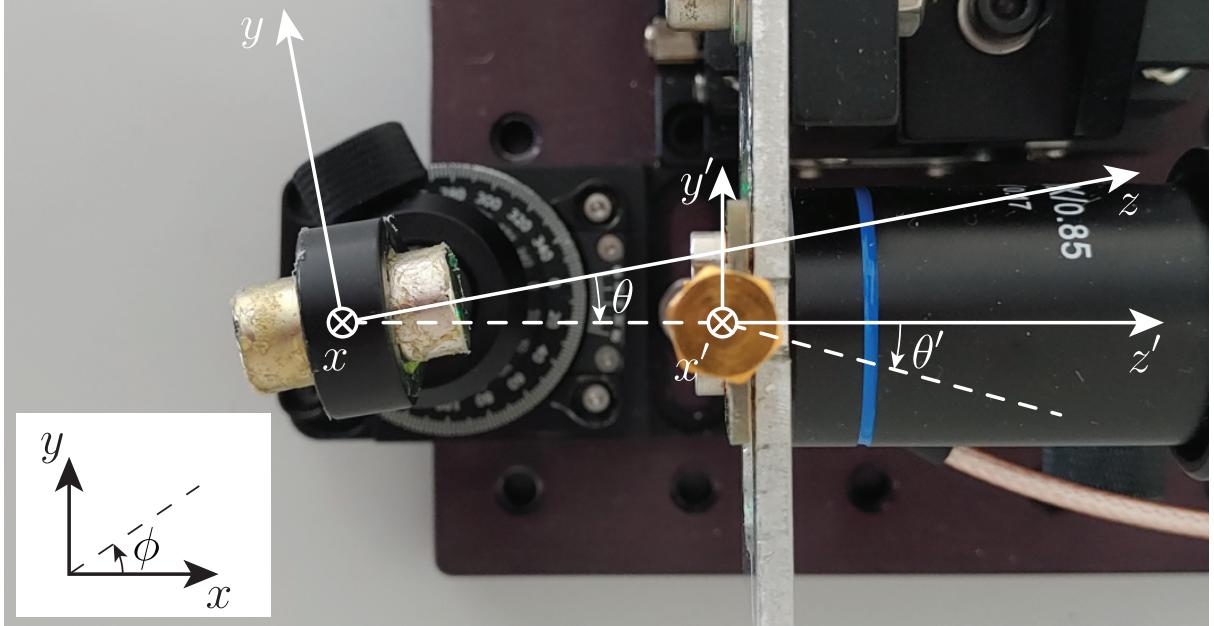


**Figure 6:** Top-down view of the setup for varying the angle of the magnet, with the coordinate systems in overlay. The  $x$ - and  $x'$ -axes point into the plane. Inset: definition of the angle  $\phi$ . In the diamond coordinate frame,  $\phi'$  is defined completely analogously.

### 3.3. Data analysis

Data analysis was done using Python. The code and raw data are available on GitHub: <https://github.com/lucasdekm/nvdiamond>. Below, we describe how the magnitude and direction of the magnetic field were extracted from the measured ESR frequencies.

#### 3.3.1. Magnitude of the magnetic field

The magnitude of the magnetic field,  $B$ , was calculated from the measured ESR frequencies  $f_u$  and  $f_l$  using Equation 2 for each pair of peaks. Each measured frequency has an uncertainty associated with it, expressed in terms of the standard deviation  $\sigma_u$  and  $\sigma_l$  for the frequencies  $f_u$  and  $f_l$  respectively. Since  $B = B(f_u, f_l)$ , we can compute the standard deviation of  $B$ , denoted  $\sigma_B$ , as

$$\sigma_B^2 = \left( \frac{\partial B}{\partial f_u} \right)^2 \sigma_u^2 + \left( \frac{\partial B}{\partial f_l} \right)^2 \sigma_l^2. \quad (8)$$

The partial derivatives can be found explicitly from Equation 2:

$$\frac{\partial B}{\partial f_u} = \frac{1}{2\gamma\sqrt{3}} \frac{2f_u - f_l}{\sqrt{f_u^2 + f_l^2 - f_u f_l - D^2}}$$

$$\frac{\partial B}{\partial f_l} = \frac{1}{2\gamma\sqrt{3}} \frac{2f_l - f_u}{\sqrt{f_u^2 + f_l^2 - f_u f_l - D^2}}.$$

When multiple pairs of peaks were present in the ESR spectrum, we took the average of the computed values of  $B$ . For  $n$  pairs of peaks,  $n$  values  $B_i$  ( $i = 1, 2, \dots, n$ ) can be found, each with an uncertainty  $\sigma_{B,i}$  given by Equation 8. The standard deviation of the mean, also known as the standard error SE, is then

$$SE_B^2 = \frac{1}{n^2} \sum_{i=1}^n \sigma_{B,i}^2. \quad (9)$$

This means that the uncertainty is smaller when more pairs of peaks were found.

For fitting, the `scipy.optimize.curve_fit` function from SciPy [8] was used. The fitting process is discussed in more detail in the Results and Discussion section.

### 3.3.2. Direction of the magnetic field

To identify the direction of the magnetic field, we essentially need to find all three components of the three-dimensional vector magnetic field  $\mathbf{B}$ . To do this, we wrote a function that calculates the expected resonance frequencies for a given vector magnetic field by diagonalizing the NV center spin Hamiltonian for all four possible orientations of the NV center. The code was adapted from existing MATLAB code [9]. It is explained further in the Appendix of this report. We then used the SciPy function `scipy.optimize.least_squares` [8] to fit the components by minimizing the squared difference between the calculated and measured resonance frequencies.

Initial guesses for the components in spherical coordinates were as follows. The magnitude  $B$  was taken as given by Equation 12 with parameters from the fit in Figure 9. The polar angle component  $B_\theta'$  increased linearly from  $0^\circ$  to  $90^\circ$ , which is a rough estimate based on the field lines around a magnetic dipole (Figure 4). Finally, the diamond is roughly at the same height as the magnet and the magnet rotates counterclockwise in Figure 6, so  $B_\phi'$  should be roughly  $270^\circ$ .

The field is then given in the reference frame of the diamond. It can be converted to the frame of the magnet by first calculating the Cartesian components and then using a rotation matrix:

$$\begin{pmatrix} B_z \\ B_y \end{pmatrix} = \begin{pmatrix} \cos\theta & \sin\theta \\ -\sin\theta & \cos\theta \end{pmatrix} \begin{pmatrix} B_{z'} \\ B_{y'} \end{pmatrix}, \quad (10)$$

where  $B_z$  and  $B_y$  are the z- and y-components of the field in the frame of the magnet, and  $B_{z'}$  and  $B_{y'}$  the components in the frame of the diamond.

## 4. Results and Discussion

A typical frequency spectrum for one of the measurements is shown in Figure 7. The spectrum shows dips in intensity, of which the locations correspond to the ESR frequencies. The eight dips correspond to the upper and lower frequencies  $f_u$  and  $f_l$  of the four NV center families. From our data, the zero-field splitting was confirmed to indeed be 2.87 GHz (Figure 11A in the Appendix).

In this section, we first discuss our results from computing the magnitude of the magnetic field  $B$  using Equation 2. In particular, we consider how the magnitude depends on the distance  $z$  along the magnet axis and the angle  $\theta$  with the magnet axis. Then, we discuss the results of fitting the vector magnetic field  $\mathbf{B}$  to the measured ESR frequencies for the data set where we varied the magnet angle.

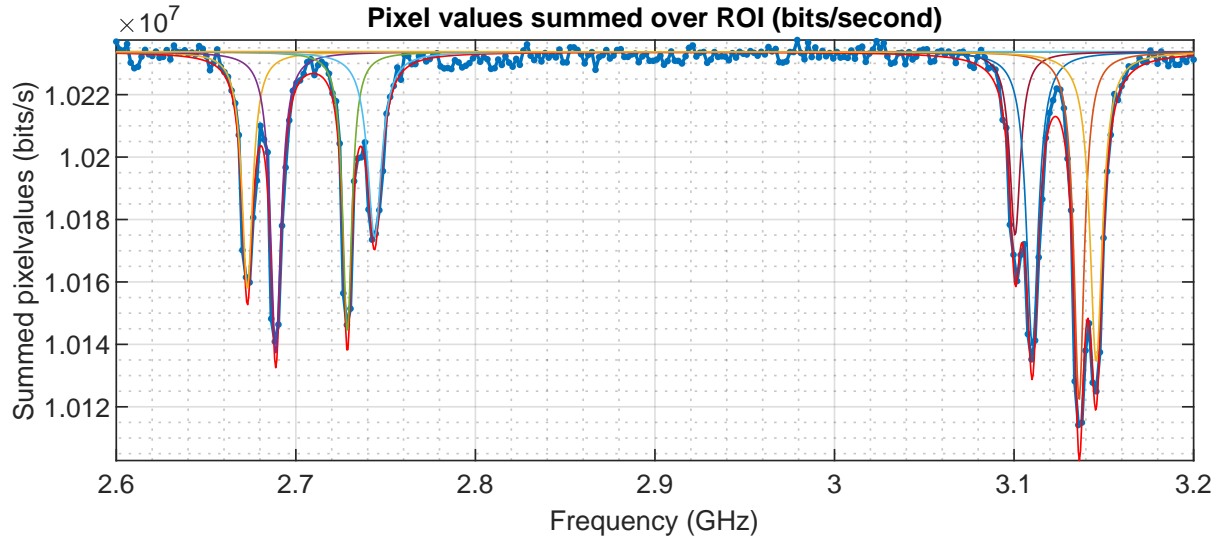


**Figure 7:** A typical frequency spectrum for an ESR frequency measurement. The vertical axis indicates the intensity of the light signal. Lorentzian fits for individual peaks are shown in a variety of colors; the red line is the sum of all these fits. This spectrum was part of the data set with varying distance along the  $z$ -axis, for  $z = 3.1$  cm.

### 4.1. Magnitude against distance

In Figure 8, the obtained magnitude of the magnetic field is plotted against the distance  $z$  between the diamond crystal and the center of the bar magnet.

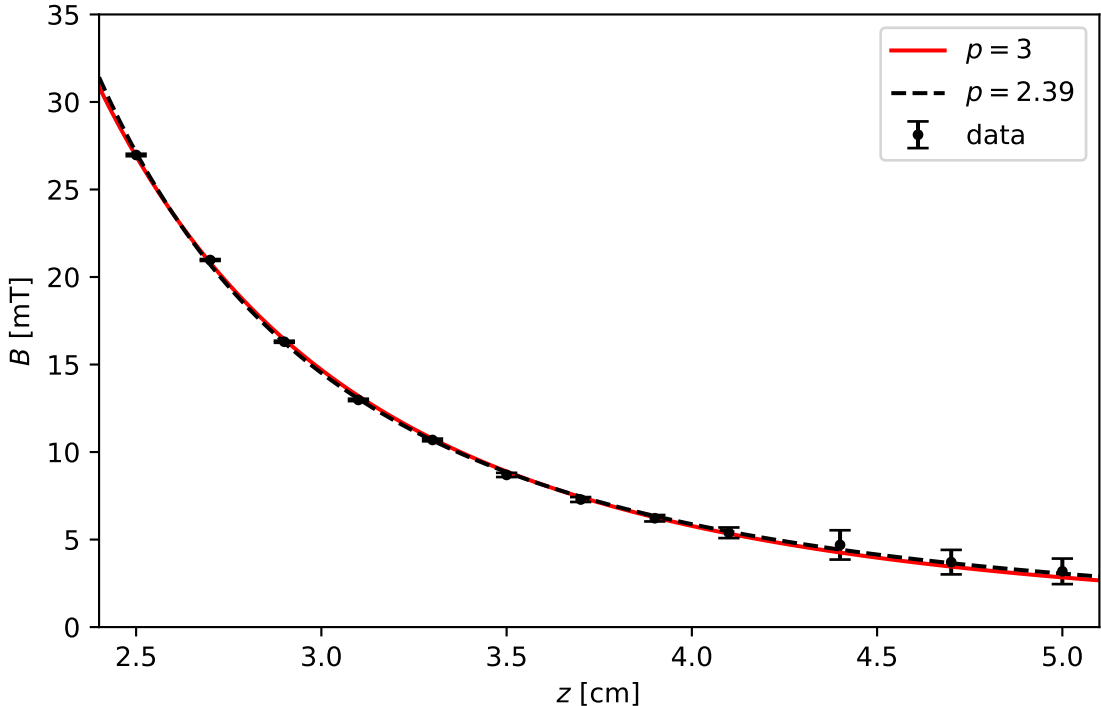


**Figure 8:** Magnitude of the magnetic field  $B$  against the distance  $z$  from the center of the magnet, along the magnet axis. Error bars indicate 3 SE (three times the standard error, i.e. the standard deviation of the mean of  $B$ ) above and below a data point. Legend indicates the parameter  $p$  for fitting according to Eq. 11.

We first fitted the data with a function

$$B(z) = C \frac{1}{(z - z_0)^p} \quad (11)$$

with  $C$ ,  $z_0$  and  $p$  fitting parameters. We introduced a translation  $z_0$  as a fitting parameter because the measurement of the initial distance using a ruler was likely to be somewhat inaccurate.

The best fit was found for  $p = 2.39$ , which is not in line with the  $1/z^3$  dependence expected from Equation 5. Moreover, for this fit,  $z_0 = 8.3$  mm. This would mean that our measurement of the initial distance was off by almost a centimeter, which is rather unlikely. Although this fit describes the data, we consider it unrealistic for this reason.

To get a better idea of whether the theory describes our data, we fixed  $p$  to be 3, leaving  $C$  and  $z_0$  as the only fitting parameters. By comparison to Equation 5, the magnetic moment can be retrieved from  $C$  as  $m = 2\pi C/\mu_0$ . As shown in Figure 8, this fit falls within three times the standard error of most data points. For this fit,  $z_0 = 2.6$  mm and  $m = 1.511 \text{ A m}^2$ . An error in the initial distance measurement of under three millimeters is reasonable, and the magnetic moment is very close to the value calculated from the manufacturer's data (Eq. 7). This shows that the data is in fact well described by the theory for an ideal magnetic dipole.

As mentioned in the Experimental Methods (Chapter 3), the ESR spectra became rather noisy at distances under 2.5 cm to the magnet center. This may be caused by the magnetic field of the physical dipole becoming less uniform at smaller distances, so that different NV centers in the diamond crystal experience a slightly different magnetic field.

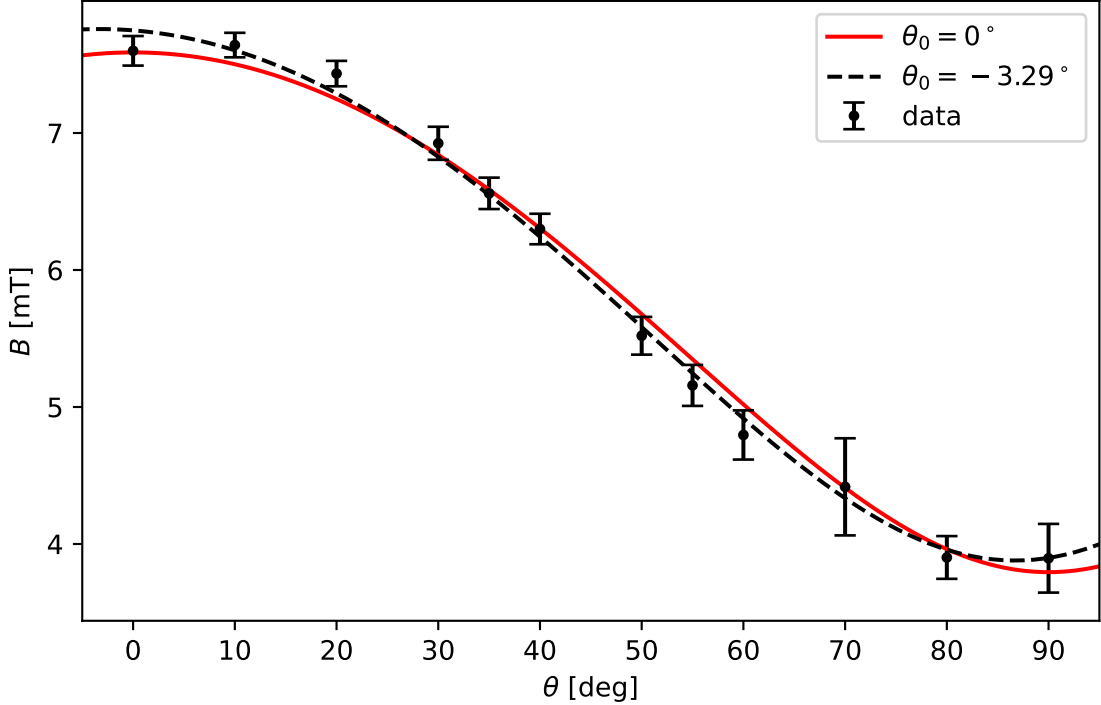


**Figure 9:** Magnitude of the magnetic field  $B$  against the angle  $\theta$  to the magnet axis, at a fixed distance  $R$  of roughly 3.2 cm to the center of the magnet. Error bars indicate 3 SE above and below a data point. Legend indicates  $\theta_0$  for the fits described by Eq. 12, in degrees. The best fit for  $\theta_0 = 0^\circ$  gave  $R_0 = -2.1$  mm; the best fit with  $\theta_0$  free was found for  $\theta_0 = -3.29^\circ$  and  $R_0 = -1.9$  mm.

## 4.2. Magnitude against angle

Figure 9 shows  $B$  for the data set where the magnet was rotated by an angle  $\theta$  at a fixed distance  $R$  from the magnet center. In accordance with Equation 6, we fitted the data with the function

$$B(\theta) = \frac{m\mu_0}{4\pi(R - R_0)^3} \sqrt{3 \cos^2(\theta - \theta_0) + 1}. \quad (12)$$

Here,  $m$  was taken to be  $1.511 \text{ A m}^2$ , as obtained by fitting the distance data. This leaves  $R_0$  and  $\theta_0$  as fitting parameters to account for inaccuracies in the measurement of the initial distance and the initial angle, respectively.

Two fits are shown in Figure 6: one with  $\theta_0$  fixed at  $0^\circ$ , and the other with the optimal fitting value for  $\theta_0$ . A slight shift of  $\theta_0 = -3.29^\circ$  gives a fit that falls within three standard errors from most data points. This can be attributed to the fact that we could not mount the magnet stage perfectly perpendicularly to the magnet. For both  $\theta_0 = 0^\circ$  and the optimal  $\theta_0 = -3.29^\circ$  fit,  $R_0$  is roughly two millimeters, which is reasonably within the expected error margins for the ruler measurement. Again, the theory explains our data well.

## 4.3. Direction

The projection on the  $(z, y)$ -plane of the fitted magnetic field vectors for the data set with varying angle is shown in Figure 10. The position of each vector corresponds to the location

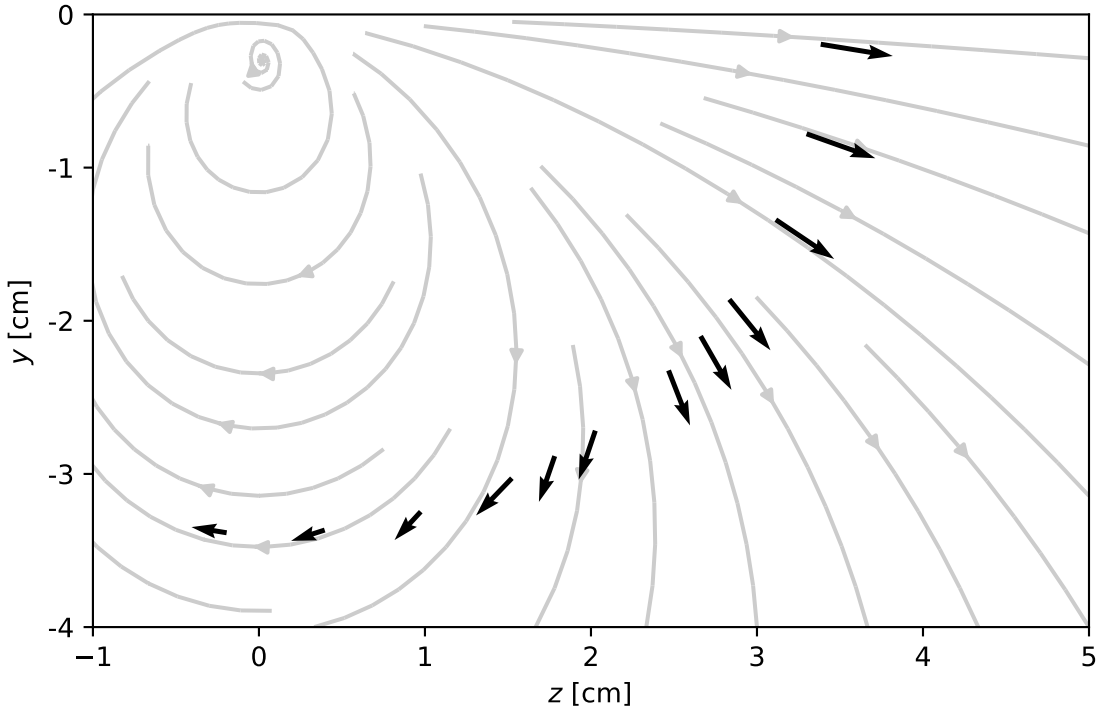


**Figure 10:** Fitted magnetic field vectors (black) and theoretical field lines (light gray). The positions of the vectors are given by the location of the diamond with respect to the magnet at the time of measurement. When computing the location, we included the corrections  $R_0$  and  $\theta_0$  as found from the fit in Figure 9. The theoretical field lines were calculated using Equation 4 with  $\mathbf{m} = 1.511\hat{\mathbf{z}}$  (in  $\text{A m}^2$ ), as found from the fit in Figure 8.

of the diamond in the reference frame of the magnet at the time of measurement. For comparison, the field lines for an ideal dipole are shown as well. The  $x$ -component is small and does not show a particular trend – it is plotted in the Appendix (Figure 11B).

The fitted  $B$ -field corresponds quite well to the theoretical field lines. However, it is worth noting that the fitting results were highly dependent on the initial guesses for the components. Results can vary for different guesses (see Figure 11C in the Appendix). Arguably, we introduced a bias by using guesses based on the expected result.

## 5. Conclusion

The aim of this project was to characterize the magnetic field of a small permanent magnet using the spin of NV centers in diamond. In particular, we studied how the magnitude of the magnetic field depends on the distance from the magnet along the magnet axis, and on the angle when going around the magnet. We also extracted the full vector magnetic field.

Computing the magnitude of the magnetic field directly from the electron spin resonance (ESR) frequencies (Equation 2) proved to be a reliable method, with a straightforward way to calculate uncertainties. The measured dependence of magnitude on distance and angle corresponded well to the prediction from classical electromagnetism.

On the other hand, fitting the components of the vector magnetic field to the ESR frequencies was highly dependent on the initial guesses. Nevertheless, for appropriate guesses, the fitted magnetic field was very similar to the field calculated from the theory.

The largest sources of uncertainty in our data came from the inaccurate ruler measurements of the distance between the magnet and the diamond. Also, the initial angle when rotating the magnet was not exactly zero degrees, and it was difficult to make sure that the magnet was fixed at the same height as the diamond crystal. By adjusting the setup, it might be possible to eliminate these inaccuracies in the future. Equation 8 can then be used to fit with  $z_0 = 0$ , which may make it possible to get a better estimate of  $p$  from the fit.

With the aforementioned inaccuracies eliminated, it may be more feasible to measure at smaller distances between the magnet and the diamond as well. Investigating the behavior of the magnetic field close to the magnet is interesting, as the field of a physical dipole may deviate from the field of an ideal dipole [6].

Aside from improving the setup, future studies may also look into improving the fitting procedure for fitting the components of the vector magnetic field. By somehow avoiding local minima, it could be possible to obtain an accurate fit even without close guesses.

## References

- [1] J. Taylor, P. Cappellaro, L. Childress, L. Jiang, D. Budker, P. Hemmer, A. Yacoby, R. Walsworth, and M. Lukin. High-sensitivity diamond magnetometer with nanoscale resolution. *Nature Physics*, 4(10):810–816, 2008.
- [2] J.-H. Storm, P. Hömmen, D. Drung, and R. Körber. An ultra-sensitive and wideband magnetometer based on a superconducting quantum interference device. *Applied Physics Letters*, 110(7):072603, 2017.
- [3] A. Kuwahata, T. Kitaizumi, K. Saichi, T. Sato, R. Igarashi, T. Ohshima, Y. Masuyama, T. Iwasaki, M. Hatano, F. Jelezko, et al. Magnetometer with nitrogen-vacancy center in a bulk diamond for detecting magnetic nanoparticles in biomedical applications. *Scientific reports*, 10(1):1–9, 2020.
- [4] L. Pham, N. Bar-Gill, D. Sage, A. Stacey, M. Markham, D. Twitchen, M. Lukin, and R. Walsworth. Enhanced metrology using preferential orientation of nitrogen-vacancy centers in diamond. *Physical Review B*, 86, 07 2012. doi: 10.1103/PhysRevB.86.121202.
- [5] *Magnetometry with spins in diamond*. TU Delft. URL: <https://magnetometryrp.quantumtinkerer.tudelft.nl/>.
- [6] D. J. Griffiths. *Introduction to Electrodynamics, Fourth edition*. Pearson, Boston, 2013.
- [7] *Technisch specificatieblad artikel S-10-20-N*. Supermagnete, 2015. URL: [www.supermagnete.nl/data\\_sheet\\_S-10-20-N.pdf](http://www.supermagnete.nl/data_sheet_S-10-20-N.pdf).
- [8] P. Virtanen, R. Gommers, T. E. Oliphant, M. Haberland, T. Reddy, D. Cournapeau, E. Burovski, P. Peterson, W. Weckesser, J. Bright, S. J. van der Walt, M. Brett, J. Wilson, K. J. Millman, N. Mayorov, A. R. J. Nelson, E. Jones, R. Kern, E. Larson, C. J. Carey, İ. Polat, Y. Feng, E. W. Moore, J. VanderPlas, D. Laxalde, J. Perktold, R. Cimrman, I. Henriksen, E. A. Quintero, C. R. Harris, A. M. Archibald, A. H. Ribeiro, F. Pedregosa, P. van Mulbregt, and SciPy 1.0 Contributors. SciPy 1.0: Fundamental Algorithms for Scientific Computing in Python. *Nature Methods*, 17:261–272, 2020. doi: 10.1038/s41592-019-0686-2.
- [9] T. Van der Sar. Personal communication, April 2021.

## Appendix

### Experimental Methods: fitting $B$ -field components

Here, we describe the Python function that we used to fit the  $B$ -field components with. Given a vector magnetic field, the function calculates the eight expected ESR frequencies.

In the diamond crystal, the NV centers can have four orientations (four ‘families’). In the matrix

$$N = \frac{1}{\sqrt{3}} \begin{pmatrix} 1 & 1 & 1 \\ 1 & 1 & -1 \\ 1 & -1 & 1 \\ -1 & 1 & 1 \end{pmatrix}, \quad (13)$$

each row is a unit vector  $\hat{\mathbf{n}}_{NV_i}$  that represents the axis of the  $i$ ’th family in Cartesian coordinates, in the frame of the diamond. Recall that the NV center Hamiltonian is given by Equation 1:

$$H = DS_{z'}^2 + \gamma \mathbf{B} \cdot \mathbf{S},$$

where the spin vector  $\mathbf{S}$  is defined in the frame of one NV center family. For a given family, the inner product  $\mathbf{B} \cdot \mathbf{S}$  can be found by decomposing the magnetic field into components parallel and perpendicular to the NV center axis. The parallel component of the vector  $\hat{\mathbf{b}} \equiv \mathbf{B}/B$  is given by the inner product with the NV center unit vector:

$$b_{||} = \hat{\mathbf{n}}_{NV_i} \cdot \hat{\mathbf{b}}. \quad (14)$$

The parallel component is then simply found as

$$b_{\perp} = \sqrt{1 - b_{||}^2}. \quad (15)$$

By symmetry in rotation about the  $z'$ -axis, we can now rewrite the Hamiltonian as

$$H = DS_{z'}^2 + \gamma B(b_{||}S_{z'} + b_{\perp}S_{y'}). \quad (16)$$

From the eigenstates of the Hamiltonian, the ESR frequencies can again be calculated, as outlined in the Theory section. When doing this for all four families, eight ESR frequencies are obtained; the function sorts the frequencies from low to high, calculates the differences with the measured ESR frequencies and outputs these differences in an array.

### Results and Discussion: zero-field splitting

The zero-field splitting  $D$  was confirmed to be approximately 2.87 GHz, as shown in Figure 11A.

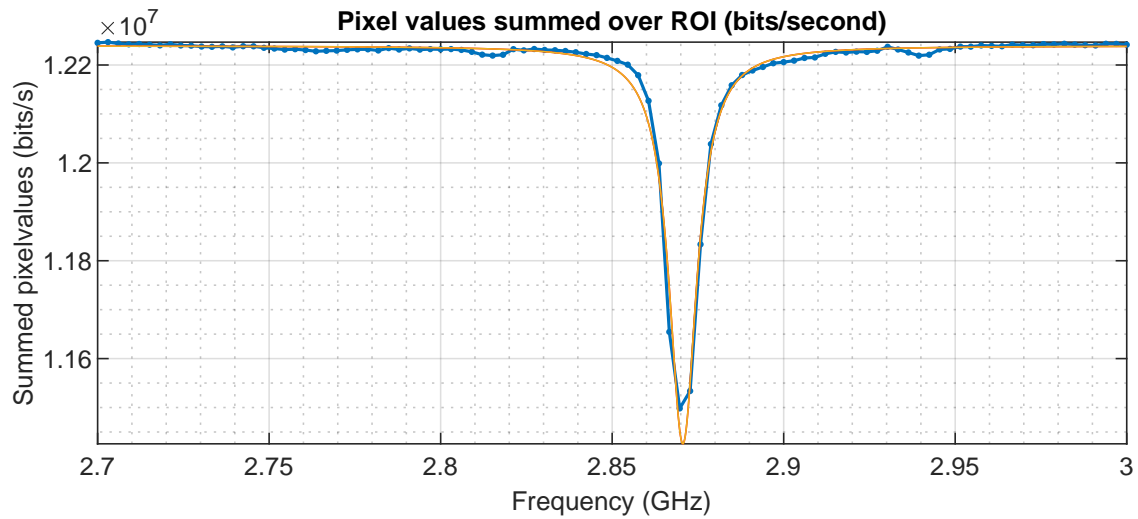
### Results and Discussion: $x$ -component of the magnetic field

The  $x$ -component of the magnetic field  $B_x$  is plotted against the rotation angle  $\theta$  of the magnet in Figure 11B.

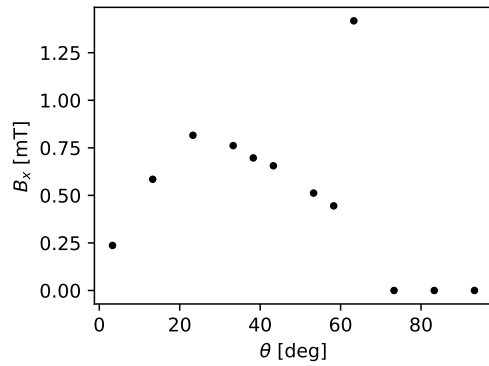
## **Results and Discussion: guesses for B-field fitting**

As mentioned, the fitting results depend strongly on the chosen guesses for the magnetic field components. To illustrate this, consider Figure 11C, where the guess for  $B_\theta$  was zero for all data points, rather than linearly increasing from 0 to  $\pi$  as in Figure 10. This produces unexpected results when the diamond is positioned almost perpendicularly to the magnet axis.

A



B



C

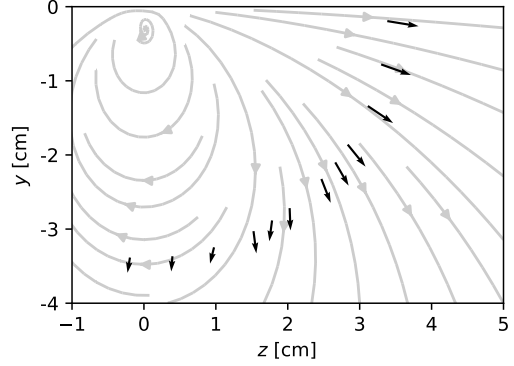


**Figure 11:** **A:** Measured frequency spectrum for no external magnetic field (no permanent magnet nearby), showing the zero-field splitting  $D \approx 2.87$  GHz. **B:**  $x$ -component of the magnetic field in the frame of the magnet against the angle  $\theta$  of the diamond w.r.t. the magnet axis. **C:** Fitted magnetic field vectors (black) and theoretical field lines (light gray). Everything was done in the same way as for Figure 10, but the guess for  $B_{\theta'}$  was changed to be zero for all data points.